Park et al. *NPG Asia Materials* (2020) 12:38
https://doi.org/10.1038/s41427-020-0219-6

NPG Asia Materials

ARTICLE Open Access

Interfacial atomic layers for full emergence of interfacial Dzyaloshinskii–Moriya interaction

Yong-Keun Park[1,2], Joo-Sung Kim[1], Yune-Seok Nam[1], Seyyoung Jeon[1], Jung-Hyun Park[1], Kyoung-Whan Kim[2], Hyun-Woo Lee[3], Byoung-Chul Min[2] and Sug-Bong Choe[1]

Abstract

Interfacial phenomena play decisive roles in modern science and technology as the scale of the material shrinks down to a few atomic layers. Such minute nanostructures require a more comprehensive understanding beyond the conventional concepts of interfaces and interfacial phenomena generated at interfaces. From a series of a few-atomic-layer-thick magnetic films, we experimentally demonstrate that, contrary to the common notion, interfacial phenomena require a finite thickness for their full emergence. The layer-thickness dependences reveal that the interfacial Dzyaloshinskii–Moriya interaction (DMI) begins to appear with increasing thickness, and emerges completely at a thickness of 2–3 atomic layers, at which the magnitude is maximized. This result implies that the DMI is suppressed when the "bulk" layer adjacent to the interface is thinner than the threshold thickness. The existence of the threshold thickness indicates the need to refine conventional perspectives on interfacial phenomena, and imposes the lowest structural bound and optimum thickness to maximize interfacial effects for technological applications.

Introduction

The Dzyaloshinskii–Moriya interaction (DMI) has attracted much attention because of its peculiar properties for realizing chiral spin structures in magnetic systems with broken inversion symmetry[1–10]. These chiral spin structures, such as chiral magnetic domain walls[1] and magnetic skyrmions[2], have been extensively studied as the building blocks of emerging magnetic memory and logic devices[3,4]. A sufficiently large DMI is essential for highly efficient domain-wall motion via current-induced spin–orbit torques (SOTs)[5,6], and for the topological protection of the skyrmion stability[7]. Hence, extensive efforts have been made to engineer a large DMI and understand its physical origin.

Interest in DMIs has exploded recently because of the discovery of large DMIs at the interfaces of magnetic multilayered systems[2,11–13]. By using these systems, the interfacial DMI strength can be engineered to be strong enough to demonstrate magnetic skyrmions at room temperature[2]. Beyond the original concept based on the atomic three-site anisotropic superexchange interaction with spin–orbit coupling[8,9], recent studies have suggested more comprehensive mechanisms with different governing parameters, such as the work function difference at the interface[11], orbital characteristics[12,14], charge distribution and interface dipole moment[15], and Rashba effect[16,17]. Although the most decisive parameters and mechanisms are still under debate, it is commonly accepted that the interfacial DMI has to be generated by broken inversion symmetries at the interfaces of heavy metals with large spin–orbit coupling[9,13].

Similar to other interfacial effects, it is commonly believed that the interfacial DMI arises at the interface itself, and thus, its strength average over the ferromagnetic layer is inversely proportional to the layer thickness. Therefore, a system with a thinner layer is expected to show a larger DMI strength, as observed by recent studies[18–20]. Such monotonic dependence has been

Correspondence: Sug-Bong Choe (sugbong@snu.ac.kr)
[1]Department of Physics and Institute of Applied Physics, Seoul National University, Seoul 08826, Republic of Korea
[2]Center for Spintronics, Korea Institute of Science and Technology, Seoul 02792, Republic of Korea
Full list of author information is available at the end of the article

explained by Yang et al.[21] based on the atomic-layer-resolved calculations of Pt/Co bilayers by suggesting that the interfacial DMI is generated mostly at the first nearest Co atomic layer to the interface, and thus, the DMI strength is inversely proportional to the layer thickness down to an atomic monolayer. In contrast, another atomic-layer-resolved calculation by Jia et al.[22] predicted a significant contribution of the second nearest Co atoms to the DMI in Pt/Co bilayers, resulting in a nonmonotonic dependence of the DMI strength on the layer thickness. Both studies agree that the interfacial phenomena originate from a few atomic layers near the interfaces, but the detailed contributions of each atomic layer to the DMI with the refined DMI mechanisms are still under debate.

In general cases, even at ideal interfaces with abrupt structural boundaries, the crossover between different material properties requires a finite nonzero thickness, over which the interfacial phenomena are generated. Such a crossover thickness might arise from the interactions between the conduction and orbital electrons with a redistribution of the charge and dipole moment[10,11,15], or spin chiral mechanisms with the Rashba effect[16,17], resulting in off-nearest-site atomic interactions[22] beyond the original concept of atomic interactions between the nearest sites.

Materials and methods

Sample fabrication

Two different series of films were prepared. The full-layer stacks of the films are 1.5-nm Ta/3-nm Pt/t_{Co} Co/5-nm W/2-nm AlO_x with different ferromagnetic Co-layer thicknesses (t_{Co}) in the range from 0.7 to 1.2 nm for the former Pt/Co/W films and 1.5-nm Ta/3-nm Pt/t_{Co} Co/0.6-nm Cu/5-nm W/2-nm AlO_x with different t_{Co} values in the range from 0.3 to 0.8 nm for the latter Pt/Co/Cu/W films. All samples were deposited by dc-magnetron sputtering on Si wafers with a 100-nm-thick SiO_2 layer. The lowermost Ta and uppermost AlO_x layers are employed as seed and protection layers, respectively. The AlO_x layers are formed by natural oxidation after depositing Al layers. To keep a similar film quality, the sputtering conditions were carefully maintained to be the same for all the films with an Ar working pressure of ~2 mTorr and sputtering power of ~10 W. To measure the maximum strength of the SOT efficiency (ε_0) and DMI-induced effective magnetic field (H_{DMI}), 20-μm-wide and 350-μm-long microwires were patterned by photolithography and ion-milling processes. To inject electric current into the microwires, 5/100-nm-thick Cr/Au electrodes were deposited by a lift-off process.

Sample characterization

The magnetic anisotropy field (H_K) and saturation magnetization (M_S) were measured by means of a vibrating sample magnetometer, where H_K and M_S were estimated by the saturation magnetic field and moment from hard- and easy-axis hysteresis loops, respectively. One can then obtain effective perpendicular magnetic anisotropy (K_U^{eff}) from the relation $K_U^{eff} = \mu_0 M_S H_K/2$. The measured M_S and H_K and estimated K_U^{eff} are listed in Supplementary Table 1.

The values of H_{DMI} and ε_0 were quantified by a measurement scheme[11] based on the variation in the SOT efficiency (ε) with respect to the in-plane magnetic field (H_x). In this scheme, a domain wall was first created in a magnetic microwire, and then, a domain-wall depinning field (H_{dep}, in the direction perpendicular to the film plane) from the initial position was detected by sweeping the external magnetic field. By measuring H_{dep} under the application of several different current densities (J), one can obtain ε via the relations $\mu_0 H_{dep}(J) = \mu_0 H_{dep}^0 + \varepsilon J$, where H_{dep}^0 is the depinning field without an electric current, and εJ corresponds to the effective magnetic field (H_{eff}, in the direction perpendicular to the film plane) caused by the SOT. By repeating these procedures by sweeping H_x, one can obtain an ε–$\mu_0 H_x$ plot, as shown in Fig. 1.

Under the application of an electric current, the damping-like SOT generates the effective magnetic field in the direction of $\hat{m} \times \hat{s}$, where $\hat{m}$ is the unit vector of the magnetization inside the domain wall and $\hat{s}$ is the unit vector of the spins associated with the SOT[23]. For the case that J is parallel to the x axis, $\hat{s}$ is parallel to the y axis, and therefore, H_{eff} along the z axis is proportional to the x component (m_x) of the magnetization inside the domain wall, i.e., $H_{eff}\hat{z} \propto m_x \hat{x} \times \hat{y}$. Since $\mu_0 H_{eff} = \varepsilon J$, one can then obtain the relation $\varepsilon \propto m_x$. By sweeping H_x, the domain wall varies from one Néel-type configuration ($m_x = -1$) to another ($m_x = 1$) through a Bloch-type configuration ($m_x = 0$). Therefore, the $\varepsilon - \mu_0 H_x$ plots exhibit the typical behavior of two saturation regimes with the Néel-type domain-wall configurations ($\varepsilon = \pm\varepsilon_0$) across the Bloch-type domain-wall configuration ($\varepsilon = 0$). Since the Bloch-type domain-wall configuration appears when H_x exactly compensates for H_{DMI} (i.e., $H_x + H_{DMI} = 0$), the x intercept (i.e., $\varepsilon = 0$) indicates the magnitude of H_{DMI} (black vertical line), as shown in Fig. 1. In addition, ε_0 is quantified from the saturation values in the Néel-type domain-wall configurations.

Results and discussion

Observation of quick DMI decay with decreasing Co-layer thickness

To demonstrate the existence of a finite thickness for DMI generation, we experimentally examined the DMI strength with respect to t_{Co}. Figure 2 summarizes the measured values of H_{DMI} (a) and ε_0 (b) obtained from the plot in Fig. 1 with respect to t_{Co}. The measured H_{DMI} and

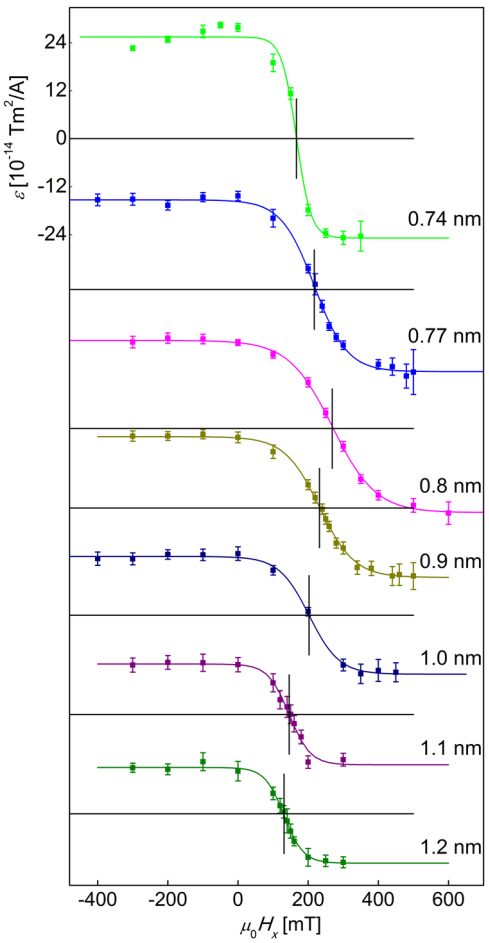

Fig. 1 Plots of ε with respect to $\mu_0 H_x$ for the series of Pt/Co/W films with different t_{Co} as indicated. The vertical error bars are the standard deviation of several repeated measurements. The black vertical lines indicate the antisymmetric center with $\varepsilon = 0$ for each curve. The curved solid lines guide the eyes.

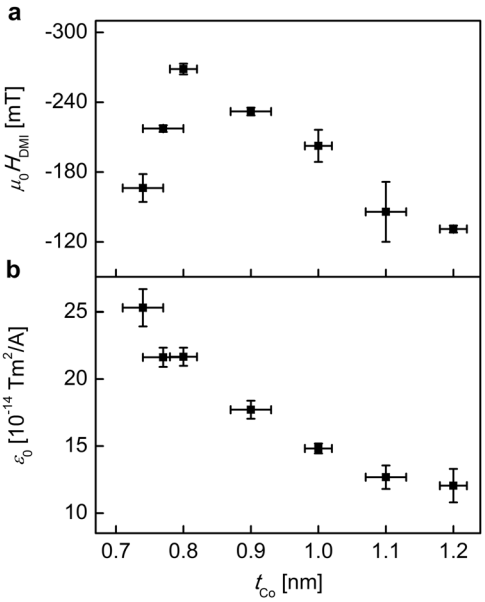

Fig. 2 Plot of H_{DMI} and ε_0 with respect to t_{Co} for the series of Pt/Co/W films. a Plot of $\mu_0 H_{DMI}$ with respect to t_{Co}. **b** Plot of ε_0 with respect to t_{Co}. The horizontal error bars correspond to the experimental accuracy of the Co-layer thickness, and the vertical error bars are the standard deviation of several repeated measurements.

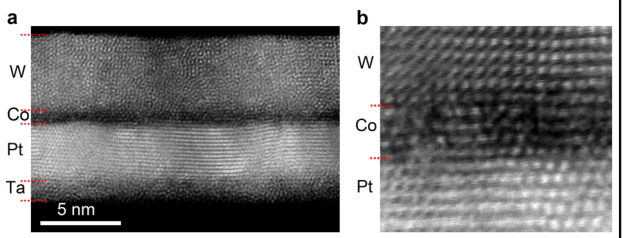

Fig. 3 Cross-sectional transmission electron microscopy image of the interfacial atomic layers. a Wide-range image of the Pt/Co/W film with the thinnest Co layer ($t_{Co} = 0.7$ nm). **b** Image magnified on the Co layer and its interfaces.

ε_0 are listed in Supplementary Table 1. Due to the interfacial nature, it is expected that both the strengths of the DMI and SOT increase as t_{Co} decreases via an increase in the surface-to-volume ratio[6,18,19,24,25]. This expectation truly occurs for the case of the SOT, as seen in Fig. 2b, that ε_0 increases monotonically as t_{Co} decreases. However, interestingly, a quite distinct behavior occurs for the case of the DMI. Figure 2a shows that H_{DMI} quickly decays in the thinner t_{Co} regime, whereas the typical interfacial behavior of the inverse proportionality appears in the thicker t_{Co} regime. The critical thickness between these two regimes is found to be ~0.8 nm, where the maximum H_{DMI} strength is achieved.

Consideration of possible structural origins

We first examined structural imperfections as the possible origins of this peculiar behavior. Among the possible structural imperfections, the discontinuous island growth of the Co layer is not observed in our films, but rather a continuous crystalline structure of the Co layer appears in a cross-sectional transmission electron microscope (Cs-TEM), which was used to confirm the degree of the continuity and roughness at the interface. The cross-sectional image visualizes a continuous crystalline structure of the Co layer, even for the thinnest case of the Co layer, as shown in Fig. 3a, and the signaling effective magnetic layer remains continuous for this series of films. If the Co layer is discontinuous (see Supplementary Fig. 1), then there is a possibility for a reduction of the DMI strength (see Supplementary Fig. 2) due to the decreasing number of atomic pairs between Co and the atoms of the

nonmagnetic material, as described in Supplementary Information. However, a closer look indicates smooth atomic-layer boundaries and clear contrast at the interfaces, as visualized in Fig. 3b, and thus, a reduced number of atomic pairs due to a discontinuous Co layer is unlikely the major origin of the quick H_{DMI} decay.

Structural variation, such as the coherent-to-incoherent transition of crystalline structures[26,27], was also examined by the measurement of K_U^{eff} with respect to t_{Co}. The measurement results (see Supplementary Fig. 3a) indicate that the coherent-to-incoherent transition occurs at approximately $t_{Co} \sim 1.2$ nm, which is very different from the critical thickness for quick H_{DMI} decay. In addition, K_U^{eff} exhibits a gradual thickness dependence that is dissimilar to the peculiar H_{DMI} variation. Hence, the coherent-to-incoherent transition associated with the K_U^{eff} variation is unlikely to share the origin of the quick H_{DMI} decay.

To check whether the quick H_{DMI} decay is possibly caused by a reduction of the magnetically effective thickness $\left(t_{Co}^{m}\right)$ near the interface, we examined the reduced amount of t_{Co}^{m} with respect to the deposited thickness t_{Co}. If W atoms penetrate into the Co layer, then they may alter the properties of the Co layer nearby, forming a reduced thickness (δ) or the so-called dead layer. Even for the continuous Co layers, there may be the possibility of a reduced number of atomic pairs effectively by the penetration of W atoms. For this test, M_S was measured by means of a vibrating sample magnetometer. Figure 4a shows the results by plotting $M_S t_{Co}$ with respect to t_{Co}. The linear dependence between $M_S t_{Co}$ and t_{Co} manifests that most of the films have similar M_S values, considering the magnetic layer volume from t_{Co}^{m}, as shown in other experiments with Pt/Co trilayer systems[28]. Then, as guided by the blue linear line of the best fit, the nonzero x intercept indicates the amount of δ, which is quantified as $\sim 0.26 \pm 0.01$ nm. Notably, δ is noticeably smaller than the critical thickness for the quick H_{DMI} decay. In addition, the roughness/mixing does not exceed the effective magnetic layer thickness (approximately two atomic layers for this sample), as shown in Fig. 3. This situation is similar to the situation depicted on the right side in Supplementary Fig. 1a, with a continuous Co layer even if the W atom penetrates into the Co layer to some extent. Therefore, the results indicate that the mechanism associated with the δ fomation is not directly responsible for the quick H_{DMI} decay.

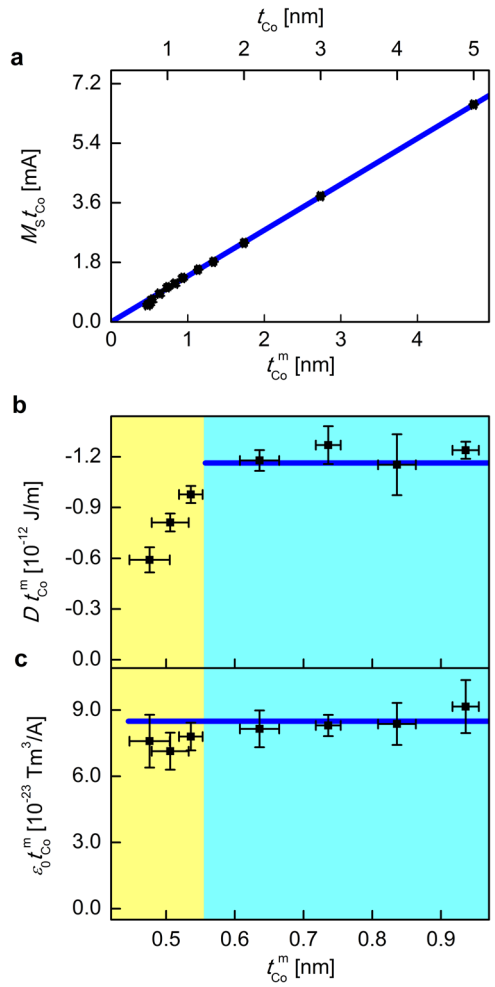

Fig. 4 Plot of $M_S t_{Co}$, $D t_{Co}$, and $\varepsilon_0 t_{Co}$ with respect to t_{Co} for the series of Pt/Co/W films. a Plot of $M_S t_{Co}$ with respect to t_{Co} (upper label) and t_{Co}^{m} (lower label). The blue line shows the linear fit. The x intercept for t_{Co} indicates δ. **b** Plot of $D t_{Co}^{m}$ with respect to t_{Co}^{m}. The blue and yellow shaded areas show the thicker and thinner t_{Co} regimes, respectively. The blue horizontal line shows the average value over the thicker t_{Co} regime. **c** Plot of $\varepsilon_0 t_{Co}^{m}$ with respect to t_{Co}^{m}. The blue horizontal line shows the average value over both regimes. In all the plots, the horizontal error bars are the experimental accuracy of the Co-layer thickness, and the vertical error bars are the standard deviation of several repeated measurements.

Analysis with the magnetically effective thickness

To obtain detailed insights into the origin more quantitatively, the DMI strength (D) is estimated by the relation $D = \mu_0 H_{DMI} M_S \lambda$, where μ_0 is the permeability constant and λ is the domain-wall width[5]. The measured D values are listed in Supplementary Table 1. The values of λ are estimated by the equation of the Bloch-type domain-wall width[5,29]; i.e., $\lambda = \left(A_{ex}/K_U^{eff}\right)^{1/2}$ under the assumption that the exchange stiffness (A_{ex}) remains constant (=22 pJ/m). We also confirmed that the possible variation in A_{ex} with respect to ferromagnetic layer thickness[29] does not change the main trend in the D variation. Then, D is analyzed in terms of t_{Co}^{m} ($=t_{Co}-\delta$). The inverse proportionality between D and t_{Co}^{m} is examined by plotting $D t_{Co}^{m}$ with respect to t_{Co}^{m}, as

shown in Fig. 4b. This scaled plot is useful for decomposing the surface contribution (D_S) and the volume contribution (D_V) via the relation $Dt_{Co}^m = D_S + D_V t_{Co}^m$. Interestingly, the plot again exhibits two different regimes. In the thicker t_{Co}^m regime (blue area), Dt_{Co}^m shows a negligible variation with respect to t_{Co}^m, indicating that D has a negligible volume contribution, i.e., $D_V \cong 0$. Therefore, the surface contribution is mostly responsible for the DMI, i.e., $Dt_{Co}^m \cong D_S$. In addition, the saturation values of Dt_{Co}^m show that D_S is fully generated in this regime, resulting in the inverse proportionality between D and t_{Co}^m.

On the other hand, in the thinner t_{Co}^m regime (yellow area), Dt_{Co}^m becomes smaller than the saturation value. The critical thickness between these two regimes is ~0.55 nm (≅3 atomic layers), which is consistent with the prediction based on the atomic-layer-resolved calculation by Jia et al.[22]. Notably, the other atomic-layer-resolved calculation by Yang et al.[21] can be extended to explain such insufficient DMI generation for the case of an incomplete atomic interface formation with large vacancies (see Supplementary Information), although this case is unlikely for our films with reasonably clear atomic-layer boundaries, as shown in Fig. 3b. It is not easy to quantify the exact contributions of these mechanisms, but both cases suggest that the incomplete generation of the interfacial DMI might be a possible origin of the quick DMI decay in the thinner regime.

The distinct thickness dependences of the DMI and SOT provide another hint to understand the interfacial and bulk phenomena, and the possibility of the independent engineering of the DMI and SOT. In contrast to the DMI that should be generated near the interfaces, the SOT is known to have two sources: at the interfaces via the Rashba effect[30] known as the source of the field-like torque, and from the adjacent nonmagnetic layers via the spin-Hall effect[24,31] known as the source of the damping-like torque. The plot of $\varepsilon_0 t_{Co}^m$ with respect to t_{Co}^m (Fig. 4c) shows that $\varepsilon_0 t_{Co}^m$ remains unchanged within the error bars over the whole thickness range. The slight reduction in $\varepsilon_0 t_{Co}^m$ with respect to t_{Co}^m might be attributed to the decrease in spin current absorption in Co as t_{Co}^m becomes too thin[32]. This observation indicates that the SOT is less sensitive to interface formation in our samples, and thus, the damping-like torque is the main source of the SOT originating mainly from the spin-Hall current from the outer nonmagnetic layers in these films. Unlike the SOT in our samples, the DMI is sensitive to the thickness of the atomic layers in the vicinity of the interface, indicating that the quick DMI decay might be attributed not only to the interface characteristics, but also to incomplete DMI generation with Co layers thinner than the critical thickness.

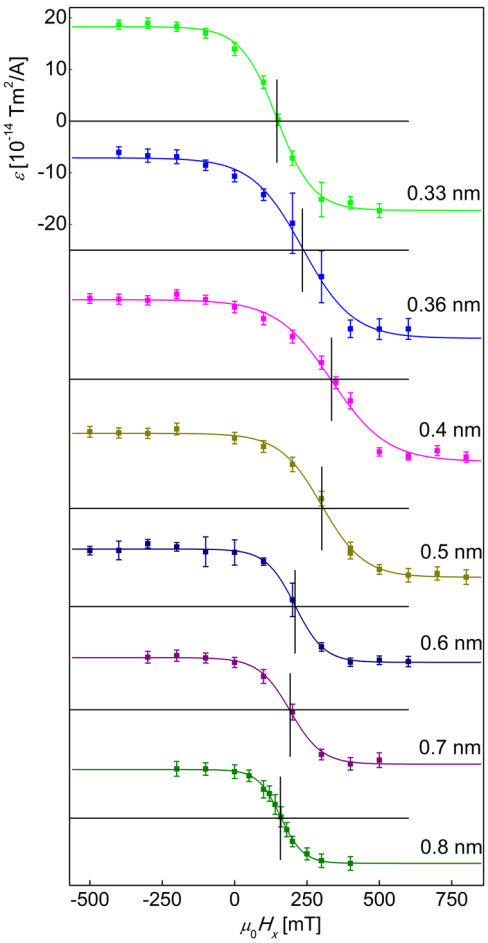

Fig. 5 Plots of ε with respect to $\mu_0 H_x$ for the series of Pt/Co/Cu/W films with different t_{Co} as indicated. The vertical error bars are the standard deviation of several repeated measurements. The black vertical lines indicate the antisymmetric center with $\varepsilon = 0$ for each curve. The curved solid lines guide the eyes.

Confirmation with other series films without a reduction of the magnetically effective thickness

To avoid any possible artifacts associated with the mechanisms of the t_{Co}^m reduction, another series of films with Pt/Co/Cu/W stacks was prepared with different t_{Co} values. In these films, a Cu layer (0.6 nm) was inserted at the Co/W interface to suppress intermixing between the Co and W atoms[33]. The same measurements were performed on Pt/Co/Cu/W samples, and the measured parameters are listed in Supplementary Table 2. The Co thickness dependence of K_U^{eff} in the Pt/Co/Cu/W samples is similar to that of the Pt/Co/W samples, as is also shown in Supplementary Fig. 3b. The same typical ε variation with respect to H_x was observed from this series of films, as shown in Fig. 5.

Figure 6a shows a plot of $M_S t_{Co}$ with respect to t_{Co} for this series of films. It is noteworthy that the x intercept of

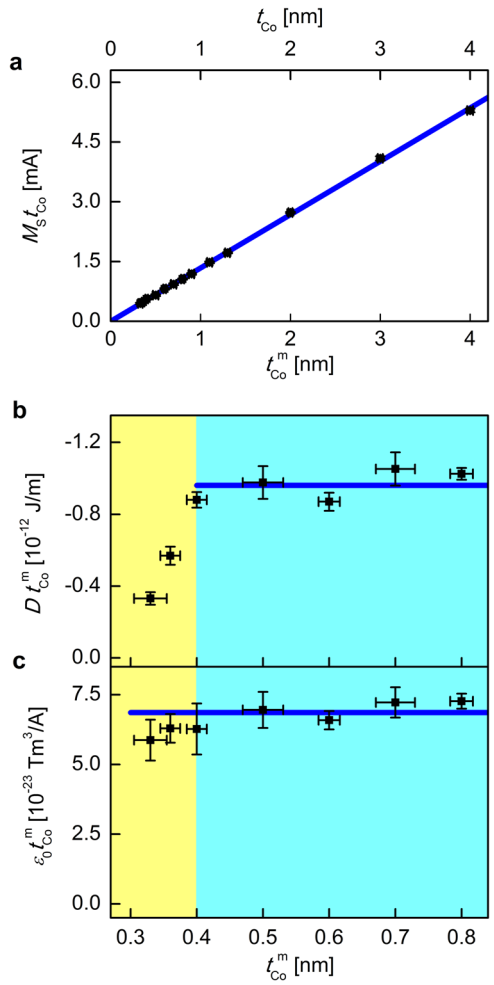

Fig. 6 Plot of $M_S t_{Co}$, Dt_{Co}, and $\varepsilon_0 t_{Co}$ with respect to t_{Co} for the series of Pt/Co/Cu/W films. a Plot of $M_S t_{Co}$ with respect to t_{Co} (upper label) and t_{Co}^m (lower label). The blue line shows the linear fit. The *x* intercept for t_{Co} indicates δ. **b** Plot of Dt_{Co}^m with respect to t_{Co}^m. The blue and yellow shaded areas show the thicker and thinner t_{Co} regimes, respectively. The blue horizontal line shows the average value over the thicker t_{Co} regime. **c** Plot of $\varepsilon_0 t_{Co}^m$ with respect to t_{Co}^m. The blue horizontal line shows the average value over both regimes. In all the plots, the horizontal error bars are the experimental accuracy of the Co-layer thickness, and the vertical error bars are the standard deviation of several repeated measurements.

the linear fit passes close to the origin, indicating that δ is negligibly small, and thus, $t_{Co}^m \cong t_{Co}$ in these films. Due to the negligibly small δ, this series of films maintains strong perpendicular magnetic anisotropy, even for films with the thinnest t_{Co} down to ~1.5 atomic monolayers. Then, the DMI and SOT are quantified by repeating the same analysis on the data in Fig. 5 as done for the former series of films. The results are shown in Fig. 6b, c with respect to t_{Co}^m. Interestingly, the figures again reproduce the distinct thickness dependence between the DMI and SOT; specifically, the interfacial DMI drops quickly in the thinner t_{Co}^m regime below 0.4 nm, whereas the SOT remains unchanged over the whole t_{Co}^m range. The same behaviors exist for both cases with and without the t_{Co}^m reduction, which confirms that the peculiar thickness dependence of the DMI is not associated with the mechanisms of the t_{Co}^m reduction.

In summary, we demonstrate the existence of a finite thickness for full DMI generation at interfaces from two different series of films Pt/Co/W and Pt/Co/Cu/W with various Co-layer thicknesses. Both series of films exhibit the same behavior of quick DMI decay with a decrease in the ferromagnetic layer thickness below a threshold thickness. Such a quick DMI decay has to be caused by insufficient DMI generation at interfaces with ferromagnetic layers that are thinner than the threshold. Therefore, the full emergence of the interfacial DMI requires a finite-threshold thickness, in contrast to the commonly accepted concept that the interfacial phenomena are generated exactly at the interfaces. Interestingly, both series of films provide a similar threshold thickness of ~2–3 atomic layers, signaling the possibility of common key mechanisms for DMI generation. These results provide a technological criterion to optimize the DMI strength with a maximum at the threshold thickness. In addition, the distinct behaviors between the DMI and SOT manifest that the DMI is generated in the vicinity of the interface, whereas the SOT is generated mainly by the spin-Hall current from the outer nonmagnetic layers in our series of films. These distinct behaviors provide the perspective of a systematic study on the interfacial DMI and bulk SOT phenomena, providing a method for the independent tuning of the DMI and SOT for spintronic applications.

Acknowledgements
This work was supported by the Samsung Science & Technology Foundation (SSTF-BA1802-07, SSTF-BA1501-07) and the National Research Foundations of Korea (NRF) funded by the Ministry of Science, ICT (MSIT) (2015M3D1A1070465). Y.-K.P., K.-W.K., and B.-C.M. were supported by the KIST Institutional Program (No. 2E29410) and the National Research Council of Science & Technology (NST) (No. CAP-16-01-KIST).

Author details
[1]Department of Physics and Institute of Applied Physics, Seoul National University, Seoul 08826, Republic of Korea. [2]Center for Spintronics, Korea Institute of Science and Technology, Seoul 02792, Republic of Korea. [3]Department of Physics, Pohang University of Science and Technology, Pohang 37673, Republic of Korea

Conflict of interest
The authors declare that they have no conflict of interest.

Supplementary information is available for this paper at https://doi.org/10.1038/s41427-020-0219-6.

Received: 2 December 2019 Revised: 25 February 2020 Accepted: 1 April 2020.
Published online: 12 June 2020

References

1. Kim, D.-Y., Kim, D.-H., Moon, J. & Choe, S.-B. Determination of magnetic domain-wall types using Dzyaloshinskii-Moriya interaction-induced domain patterns. *Appl. Phys. Lett.* **106**, 262403 (2015).
2. Woo, S. et al. Current-driven dynamics and inhibition of the skyrmion Hall effect of ferromagnetic skyrmions in GdFeCo films. *Nat. Commun.* **9**, 959 (2018).
3. Parkin, S. S. P. & Yang, S.-H. Memory on the racetrack. *Nat. Nanotech.* **10**, 195–198 (2015).
4. Fert, A., Cros, V. & Sampaio, J. Skyrmions on the track. *Nat. Nanotech.* **8**, 152–156 (2013).
5. Thiaville, A., Rohart, S., Jué, É., Cros, V. & Fert, A. Dynamics of Dzyaloshinskii domain walls in ultrathin magnetic films. *Europhys. Lett.* **100**, 57002 (2012).
6. Franken, J. H., Herps, M., Swagten, H. J. M. & Koopmans, B. Tunable chiral spin texture in magnetic domain-walls. *Sci. Rep.* **4**, 5248 (2014).
7. Sampaio, J., Cros, V., Rohart, S., Thiaville, A. & Fert, A. Nucleation, stability and current-induced motion of isolated magnetic skyrmions in nanostructures. *Nat. Nanotech.* **8**, 839–844 (2013).
8. Dzyaloshinsky, I. A thermodynamics theory of weak ferromagnetism of antiferromagnetics. *J. Phys. Chem. Solid.* **4**, 241–255 (1958).
9. Moriya, T. Anisotropic superexchange interaction and weak ferromagnetism. *Phys. Rev.* **120**, 91–98 (1960).
10. Fert, A. & Levy, P. M. Role of anisotropic exchange interactions in determining the properties of spin-glasses. *Phys. Rev. Lett.* **44**, 1538–1541 (1980).
11. Park, Y.-K. et al. Experimental observation of the correlation between the interfacial Dzyaloshinskii-Moriya interaction and work function in metallic magnetic trilayers. *NPG Asia Mater.* **10**, 995–1001 (2018).
12. Kim, S. et al. Correlation of the Dzyaloskinskii-Moriya interaction with Heisenberg exchange and orbital asphericity. *Nat. Commun.* **9**, 1648 (2018).
13. Soumyanarayanan, A., Reyren, N., Fert, A. & Panagopoulos, C. Emergent phenomena induced by spin-orbit coupling at surfaces and interfaces. *Nature* **539**, 509–517 (2016).
14. Belabbes, A., Bihlmayer, G., Bechstedt, F., Blügel, S. & Manchon, A. Hund's rule-driven Dzyaloskinskii-Moriya interaction at 3d-5d interfaces. *Phys. Rev. Lett.* **117**, 247202 (2016).
15. Belabbes, A., Bihlmayer, G., Blügel, S. & Manchon, A. Oxygen-enabled control of Dzyaloshinskii-Moriya interaction in ultra-thin magnetic films. *Sci. Rep.* **6**, 24634 (2016).
16. Kim, K.-W., Lee, H.-W., Lee., K.-J. & Stiles, M. D. Chirality from interfacial spin-orbit coupling effects in magnetic bilayers. *Phys. Rev. Lett.* **111**, 216601 (2013).
17. Kundu., A. & Zhang, S. Dzyaloshinskii-Moriya interaction mediated by spin-polarized band with Rashba spin-orbit coupling. *Phys. Rev. B.* **92**, 094434 (2015).
18. Chaurasiya, A. K. et al. Direct observation of interfacial Dzyaloshinskii-Moriya interaction from asymmetric spin-wave propagation in W/CoFeB/SiO_2 heterostructures down to sub-nanometer CoFeB thickness. *Sci. Rep.* **6**, 32592 (2016).
19. Kim., N.-H. et al. Interfacial Dzyaloshinskii-Moriya interaction, surface anisotropy energy, and spin pumping at spin orbit coupled Ir/Co interface. *Appl. Phys. Lett.* **108**, 142406 (2016).
20. Han, D.-S. et al. Asymmetric hysteresis for probing Dzyaloshinskii-Moriya interaction. *Nano Lett.* **16**, 4438–4446 (2016).
21. Yang, H., Thiaville, A., Rohart, S., Fert, A. & Chshiev, M. Anatomy of Dzyaloshinskii-Moriya interaction at Co/Pt interfaces. *Phys. Rev. Lett.* **115**, 267210 (2015).
22. Jia, H., Zimmermann, B. & Blügel, S. First-principles investigation of chiral magnetic properties in multilayers: Rh/Co/Pt and Pd/Co/Pt. *Phys. Rev. B.* **98**, 144427 (2018).
23. Emori, S., Bauer, U., Ahn, S.-M., Martinez, E. & Beach, G. S. D. Current-driven dynamics of chiral ferromagnetic domain walls. *Nat. Mater.* **12**, 611–616 (2013).
24. Emori, S. et al. Spin Hall torque magnetometry of Dzyaloshinskii domain walls. *Phys. Rev. B.* **90**, 184427 (2014).
25. Belmeguenai, M. et al. Interfacial Dzyaloshinskii-Moriya interaction in perpendicularly magnetized Pt/Co/AlO_x ultrathin films measured by Brillouin light spectroscopy. *Phys. Rev. B* **91**, 180405(R) (2015).
26. Jungblut, R., Johnson, M. T., Stegge, J., Reinders., A. & Broeder, F. J. A. Orientational and structural dependence of magnetic anisotropy of Cu/Ni/Cu sandwiches: misfit interface anisotropy. *J. Appl. Phys.* **75**, 6424 (1994).
27. Bruno, P. & Renard, J.-P. Magnetic surface anisotropy of transition metal ultrathin films. *Appl. Phys. A.* **49**, 499–506 (1989).
28. Bandiera, S., Sousa, R. C., Rodmacq, B. & Dieny, B. Asymmetric interfacial perpendicular magnetic anisotropy in Pt/Co/Pt trilayers. *IEEE Magn. Lett.* **2**, 3000504 (2011).
29. Metaxas, P. J. et al. Creep and flow regimes of magnetic domain-wall motion in ultrathin Pt/Co/Pt films with perpendicular anisotropy. *Phys. Rev. Lett.* **99**, 217208 (2007).
30. Miron, I. M. et al. Current-driven spin torque induced by the Rashba effect in a ferromagnetic metal layer. *Nat. Mater.* **9**, 230–234 (2010).
31. Hoffmann, A. Spin Hall effects in metals. *IEEE Trans. Magn.* **49**, 5172–5193 (2013).
32. Kim, K.-W. Spin transparency for the interface of an ultrathin magnet within the spin dephasing length. *Phys. Rev. B* **99**, 224415 (2019).
33. Bandiera, S., Sousa, R. C., Rodmacq, B. & Dieny, B. Enhancement of perpendicular magnetic anisotropy through reduction of Co-Pt interdiffusion in (Co/Pt) multilayers. *Appl. Phys. Lett.* **100**, 142410 (2012).